

Implementations of more general solid-state (SWAP)^{1/m} and controlled-(swap)^{1/m} gates

Wen-Qiang Liu and Hai-Rui Wei*

School of Mathematics and Physics, University of Science and Technology Beijing, Beijing 100083, China

E-mail: *hrwei@ustb.edu.cn

Abstract. Universal quantum gates are the core elements in quantum information processing. We design two schemes to realize more general (SWAP)^{1/m} and controlled-(swap)^{1/m} gates (for integer $m \geq 1$) by directing flying single photons to solid-state quantum dots. The parameter m is easily controlled by adjusting two quarter-wave plates and one half-wave plate. Additional computational qubits are not required to construct the two gates. Evaluations of the gates indicate that our proposals are feasible with current experimental technology.

1. Introduction

Quantum information processing (QIP), which exploits the quantum features of superposition and entanglement, promises to outperform its classical counterparts in solving certain computationally demanding problems in terms of security or speed [1]. Quantum computing has the potential to execute Shor's factorization algorithm [2, 3] and Grover's search algorithm [4–6], which are dramatically faster than traditional algorithms. Quantum computation allows one to build more efficient, secure, and useful quantum computers than the existing classical ones [1]. Quantum communication possesses unprecedented advantages over classical communication. It holds an arduous assignment for absolutely secure and reliable information dissemination as well as faithful transfer of unknown quantum states between distant sites.

It is well known that quantum gates are the core elements in QIP. Controlled-NOT (CNOT) gates are among the most popular universal gates and are essential for various quantum information protocols [7, 8]. (SWAP)^{1/m} gates are the cheapest and the most natural two-qubit gates, and they can be used widely in quantum computation and communication [9]. In 2008, Balakrishnan and Sankaranarayanan [10] studied the entangling character of (SWAP)^{1/m} gates. It has been shown that the (SWAP)^{1/m} family of gates is universal and as efficient as CNOT gates in terms of the required gate count in performing arbitrary two-qubit quantum operations [9]. Therefore, (SWAP)^{1/m} gates provide a way to implement quantum computation independent of CNOT gates; three (SWAP)^{1/m} gates and six single-qubit gates are sufficient and necessary to implement

arbitrary two-qubit operations [9]. Controlled-(swap) (Fredkin) gates, first introduced by Fredkin and Toffoli [11], play an important role in classical reversible computation and multi-user quantum communication [1]. Controlled-(swap) gates and Hadamard gates are competent to synthesize any multiqubit unitary operation [11]. Moreover, controlled-(swap) gates can be directly applied to error-correction [12, 13], quantum fault tolerance [14], quantum algorithms [15], fingerprinting [16, 17], optimal cloning [18], and controlled entanglement filtering.

Significant progress has been made on the (SWAP)^{1/m} family of gates in recent years. Early in 1995, Barenco *et al.* [7] proved that three CNOT gates are sufficient to implement a SWAP gate. In 2005, Fiorentino *et al.* [19] presented an interesting scheme to realize a linear-optical SWAP gate for the momentum and polarization degrees of freedom (DOFs) of a single photon. In the same year, Liang and Li [20] fulfilled the construction of a SWAP gate between a single photon and an atom. A few values of m and the corresponding entangling character of (SWAP)^{1/m} gates were proposed by Balakrishnan *et al.* [10] in 2008. Subsequently, in 2010, Koshino *et al.* [21] showed a photon-photon (SWAP)^{1/2} gate via a three-level Λ system. In 2015, Wei *et al.* [22] designed a quantum circuit to implement a solid-state (SWAP)^{1/m} gate assisted by diamond nitrogen-vacancy (NV) centers. In 2018, a passive swap operation was demonstrated based on a single photon and an atom in a material Λ -system [23], which provided a versatile building block to achieve universal quantum gates such as (SWAP)^{1/2} [24]. In 2019, Calafell *et al.* created a (SWAP)^{1/2} gate with high fidelity and success rate by employing strong two-plasmon absorption in graphene nanoribbons [25].

The optimal cost of a controlled-(swap) gate is five two-qubit entangling gates [26, 27]. In 2006, Fiurášek [28] designed a linear optical controlled-(swap) gate with 4.1×10^{-3} success probability. Subsequently, utilizing partial-SWAP gates, Fiurášek [29] presented the linear optical controlled-(swap) gate again. In 2008, Gong *et al.* [30] further improved the success probability of the controlled-(swap) gate to 1/64 based on time entanglement and linear optics. In 2016, Wei *et al.* [31] proposed a scheme of achieving a two-photon four-qubit controlled-(swap) gate via NV defect centers. In 2017, Ono *et al.* [32] experimentally demonstrated a photonic controlled-(swap) gate. Over the same period, controlled-(swap) gates were also obtained in a hybrid system comprising flying photons and atomic ensembles [33]. In 2018, Ren *et al.* [34] constructed a near-deterministic polarization-spatial hyperparallel controlled-(swap) gate with high fidelity and efficiency using NV centers in the optical cavity.

Thus far, various apparatuses have been proposed to implement QIP, and solid-state devices emerged as one of the most popular candidates among physical systems due to their good scalability, possible coherent control, and readout of the single spins. Photon-mediated interactions between solid-state matter (solid state as the quantum node and a photon as the quantum bus) are of fundamental importance in long-distance solid-state QIP [35]. Single-photon Hadamard gates [36], deterministic two-photon controlled-phase gates [37], and single-photon transports [38] were designed through atom-mediated interactions. Semiconducting quantum dots (QDs) in cavities are an

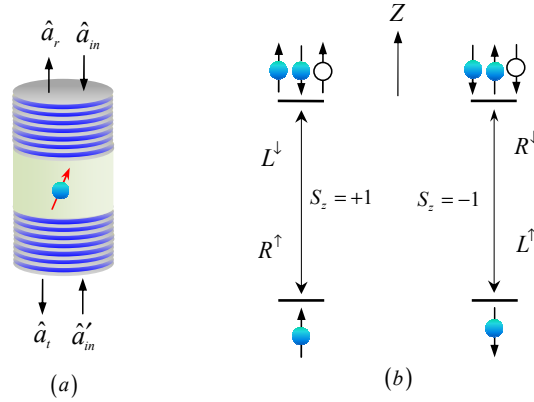


Figure 1. (Color online) (a) Structure of a singly charged QD inside a double-sided optical microcavity with a circular cross-section. (b) Energy-level scheme of a singly charged QD inside a double-sided optical microcavity with the polarization allowed transition rules for the coupling photons. $|R\rangle$ ($|L\rangle$) represents a right-circularly (left-circularly) polarized photon.

outstanding service for solid-state qubits, and remarkable progress has been achieved in QD-spin QIP. QDs could be assembled experimentally in large arrays and designed to have certain characteristics. The electronic spin confined in a charged QD supports μs coherence time [39, 40] and ps or fs time-scale single-qubit manipulations [41–44]. The manipulation and measurement of the QD spin can be achieved electrically [45] or optically [46]. Researchers have devoted much effort to the integration of charged QDs with cavities to improve photon-QD interactions. Charged QDs amalgamated with nanophotonic micropillar cavities have been experimentally demonstrated recently [47–49].

In this paper, we propose two schemes to definitively implement solid-state $(\text{SWAP})^{1/m}$ and controlled- $(\text{swap})^{1/m}$ gates for single QD qubits embedded in double-sided microcavities. The electron spins in single charged QDs serve as gate qubits, whereas flying photons act as mediated matter (bus) for bridging distant QDs. The spin-dependent phase shifts on uncoupled photons are employed to construct $(\text{SWAP})^{1/m}$ and controlled- $(\text{swap})^{1/m}$ gates. Our schemes have the following characters: (1) They are generalized and integer is $m \geq 1$; (2) the controllable parameter m can be achieved by employing two quarter-wave plates (QWPs) and one half-wave plate (HWP); (3) additional electrons are not required in the construction of the two gates; and (4) our schemes are simpler than their synthesis-based and cross-Kerr-based counterparts.

2. Solid-state $(\text{SWAP})^{1/m}$ gate

Figure 1 illustrates the structure and energy level diagram for a negatively charged QD trapped in a double-sided microcavity [50]. An excess electron is injected, and a negatively charged exciton X^- consisting of two electrons of opposite spin bounded to one heavy hole with two possible spin orientations is created by optical excitation [51]. A

qubit is encoded in two ground electron spin states $|\uparrow\rangle$ and $|\downarrow\rangle$, with angular momentum projections $J_z = \pm 1/2$. The exciton spin states are $|\uparrow\downarrow\uparrow\rangle$ and $|\downarrow\uparrow\downarrow\rangle$. Here, $|\uparrow\rangle$ and $|\downarrow\rangle$ are the heavy hole spin states with $J_z = \pm 3/2$. Because of the conservation of total spin angular momentum, the transition $|\uparrow\rangle \rightarrow |\uparrow\downarrow\uparrow\rangle$ is the resonance derived from the $S_z = +1$ circularly polarized photon, marked by R^\uparrow and L^\downarrow . $|\downarrow\rangle \rightarrow |\downarrow\uparrow\downarrow\rangle$ is the resonance originating from the $S_z = -1$ circularly polarized photon, marked by R^\downarrow and L^\uparrow . Here, R and L denote the right- and left-circularly polarized photons, respectively. The superscripts \uparrow and \downarrow of R (L) indicate that the propagation directions of the R - (L -) polarized photons are along and against the z axis, respectively.

The transmission and reflection coefficients of the incident photon are obtained by solving the Heisenberg equations of motion for cavity mode, which is driven by the corresponding input field operators \hat{a}_{in} and \hat{a}'_{in} from the top and bottom of the cavity, and from the dipole-lowering operations (i.e., \hat{a} and σ_-) [52]

$$\begin{cases} \frac{d\hat{a}}{dt} = - \left[i(\omega_c - \omega) + \kappa + \frac{\kappa_s}{2} \right] \hat{a} - g\sigma_- - \sqrt{\kappa}\hat{a}_{in} - \sqrt{\kappa}\hat{a}'_{in} + \hat{H}, \\ \frac{d\sigma_-}{dt} = - \left[i(\omega_{X^-} - \omega) + \frac{\gamma}{2} \right] \sigma_- - g\sigma_z\hat{a} + \hat{G}, \end{cases} \quad (1)$$

and the input-output relationships in the cavity are expressed as [52]

$$\hat{a}_r = \hat{a}_{in} + \sqrt{\kappa}\hat{a}, \quad \hat{a}_t = \hat{a}'_{in} + \sqrt{\kappa}\hat{a}. \quad (2)$$

We take $\langle \sigma_z \rangle = -1$; that is, a sufficiently large κ is taken by the external electrical field to ensure a weak excitation approximation throughout our operation, which is applicable to single-photon process, and even two-photon process [53]. Thus, the reflection/transmission coefficients of a realistic QD-cavity system can be written as follows [54]

$$r(\omega) = 1 + t(\omega), \quad t(\omega) = \frac{-\kappa[i(\omega_{X^-} - \omega) + \frac{\gamma}{2}]}{[i(\omega_{X^-} - \omega) + \frac{\gamma}{2}][i(\omega_c - \omega) + \kappa + \frac{\kappa_s}{2}] + g^2}. \quad (3)$$

Here, ω_c , ω , and ω_{X^-} are the resonance frequencies of the cavity mode, the input incident single-photon pulse, and the dipole transition of the negatively charged exciton X^- , respectively. g is the corresponding QD-cavity coupling strength. $\gamma/2$, κ , and $\kappa_s/2$ are defined as the decay rates of the X^- dipole, the total cavity energy, and the cavity energy leakage, respectively. \hat{H} and \hat{G} denote the noise operators related to reservoirs and are needed to conserve the commutation relations. σ_z is the inversion operator of the singly charged QD, and \hat{a}_{in} , \hat{a}'_{in} and \hat{a}_r , \hat{a}_t are the input and output field operators, respectively.

When $\kappa \gg \kappa_s$ (side leakage from the cavity is negligible), under resonance frequency condition $\omega_c = \omega = \omega_{X^-}$, the spin-dependent optical transitions can be written as [55,56]

$$\begin{aligned} |R^\uparrow \uparrow\rangle &\rightarrow |L^\downarrow \uparrow\rangle, & |R^\downarrow \uparrow\rangle &\rightarrow -|R^\downarrow \uparrow\rangle, & |R^\uparrow \downarrow\rangle &\rightarrow -|R^\uparrow \downarrow\rangle, & |R^\downarrow \downarrow\rangle &\rightarrow |L^\uparrow \downarrow\rangle, \\ |L^\uparrow \uparrow\rangle &\rightarrow -|L^\uparrow \uparrow\rangle, & |L^\downarrow \uparrow\rangle &\rightarrow |R^\uparrow \uparrow\rangle, & |L^\uparrow \downarrow\rangle &\rightarrow |R^\downarrow \downarrow\rangle, & |L^\downarrow \downarrow\rangle &\rightarrow -|L^\downarrow \downarrow\rangle. \end{aligned} \quad (4)$$

The underlying mechanism is that, for coupled photon-trion interactions, the circularly polarized photon is reflected without any phase shift, whereas for decoupled photon-trion interactions, the photon is transmitted with a π -phase shift.

Next, we utilize above spin-dependent quantum phase to construct the $(\text{SWAP})^{1/m}$ gate between two independent QD spins, see figure 2. The effect of such $(\text{SWAP})^{1/m}$ gate can be presented by the unitary matrix

$$U_{(\text{SWAP})^{1/m}} = \begin{pmatrix} 1 & 0 & 0 & 0 \\ 0 & \frac{1+e^{i\pi/m}}{2} & \frac{1-e^{i\pi/m}}{2} & 0 \\ 0 & \frac{1-e^{i\pi/m}}{2} & \frac{1+e^{i\pi/m}}{2} & 0 \\ 0 & 0 & 0 & 1 \end{pmatrix}, \quad (5)$$

in the computational $\{| \uparrow_a \uparrow_b \rangle, | \uparrow_a \downarrow_b \rangle, | \downarrow_a \uparrow_b \rangle, | \downarrow_a \downarrow_b \rangle\}$ basis.

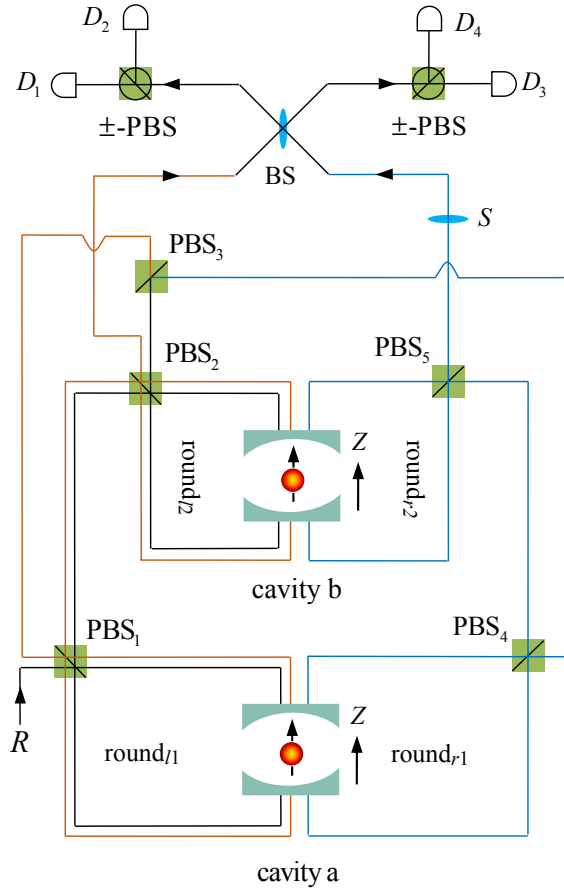


Figure 2. (Color online) Schematic diagram for the construction of a deterministic solid-state $(\text{SWAP})^{1/m}$ gate for $m \geq 1$. Each PBS represents a polarizing beam splitter in the $\{|R\rangle, |L\rangle\}$ basis transmitting the R -polarized component and reflecting the L -polarized component, respectively. \pm PBS transmits the $|+\rangle$ -polarized photon and reflects the $|-\rangle$ -polarized photon, respectively. S is a phase gate performing the operation $S = e^{i\pi/m}|R\rangle\langle R| + |L\rangle\langle L|$ on the right arm. BS stands for the balanced beam splitter. Each D denotes a single-photon polarization detector.

Firstly, suppose the two QDs are initially prepared into arbitrary normalization state

$$|\Phi_e\rangle = (\cos \alpha | \uparrow_a \rangle + \sin \alpha | \downarrow_a \rangle) \otimes (\cos \beta | \uparrow_b \rangle + \sin \beta | \downarrow_b \rangle). \quad (6)$$

For the gate operation, a single photon in state $|R_l\rangle$ is injected. The polarizing beam splitter (PBS) in the $\{|R\rangle, |L\rangle\}$ basis transmits the R -polarized component to interact with the QD_a. That is, PBS₁ transforms the state of the whole system from

$$|\Phi_{ep}\rangle_0 = |R_l\rangle \otimes (\cos \alpha |\uparrow_a\rangle + \sin \alpha |\downarrow_a\rangle) \otimes (\cos \beta |\uparrow_b\rangle + \sin \beta |\downarrow_b\rangle) \quad (7)$$

into

$$|\Phi_{ep}\rangle_1 = |R_l^\downarrow\rangle \otimes (\cos \alpha |\uparrow_a\rangle + \sin \alpha |\downarrow_a\rangle) \otimes (\cos \beta |\uparrow_b\rangle + \sin \beta |\downarrow_b\rangle). \quad (8)$$

Here, subscripts e and ep stand for the electron state and the hybrid electron-photon state, respectively. The interaction between R -polarized wave packet and QD_a induces the system from $|\Phi_{ep}\rangle_1$ to

$$|\Phi_{ep}\rangle_2 = (-\cos \alpha |R_l^\downarrow\rangle |\uparrow_a\rangle + \sin \alpha |L_l^\uparrow\rangle |\downarrow_a\rangle) \otimes (\cos \beta |\uparrow_b\rangle + \sin \beta |\downarrow_b\rangle). \quad (9)$$

Here, the subscripts l or r (mentioned later) of R^\downarrow (L^\uparrow) denote that the R^\downarrow - (L^\uparrow -) polarized component is emitted from the left or right arms, respectively (see figure 2).

From equations (6)–(9) combining with equation (4), one can see that the transformation of round_{l₁} in figure 2 can be described by a unitary matrix $U_{\text{round}_{l_1}}$,

$$U_{\text{round}_{l_1}} = \begin{pmatrix} -1 & 0 & 0 & 0 \\ 0 & 0 & 0 & 1 \\ 0 & 0 & -1 & 0 \\ 0 & 1 & 0 & 0 \end{pmatrix}, \quad (10)$$

in the $\{|R\rangle|\uparrow\rangle, |R\rangle|\downarrow\rangle, |L\rangle|\uparrow\rangle, |L\rangle|\downarrow\rangle\}$ basis.

Subsequently, the photons interact with round_{l₂}, and then the state of the system becomes

$$\begin{aligned} |\Phi_{ep}\rangle_3 = & \cos \alpha \cos \beta |R_l^\downarrow\rangle |\uparrow_a\uparrow_b\rangle - \cos \alpha \sin \beta |L_l^\uparrow\rangle |\uparrow_a\downarrow_b\rangle \\ & - \sin \alpha \cos \beta |L_l^\uparrow\rangle |\downarrow_a\uparrow_b\rangle + \sin \alpha \sin \beta |R_l^\downarrow\rangle |\downarrow_a\downarrow_b\rangle. \end{aligned} \quad (11)$$

Next, as shown in figure 2, the L -polarized components are reflected to interact with round_{r₁}, round_{r₂}, phase gate $S = e^{i\pi/m}|R\rangle\langle R| + |L\rangle\langle L|$, and 50:50 balanced beam splitter (BS) in succession. Alternatively, the R -polarized components are transmitted to round_{l₁}, round_{l₂}, and BS in succession. Before and after the photons interact with round_{r₁} and round_{r₂} (round_{l₁} and round_{l₂}), Hadamard operations H_{ea} and H_{eb} are performed on QD_a and QD_b, respectively. It is worth mentioning that the single-qubit operation performed on QD can be realized by using a ns spin resonance microwave pulse [41] or ultrafast ps (or fs) optical pulse from the cavity side [42] within the spin coherence time (20 μ s) [40]. When $(\pi/2)_y$ pulses are applied to complete H_{ea} and H_{eb} , the incident photon can be stored in optical circular or matter qubit. $S = e^{i\pi/m}|R\rangle\langle R| + |L\rangle\langle L|$ can also be actualized by employing P($\frac{2m+1}{2m}\pi$), QWP($\frac{\pi}{4}$), HWP($\frac{m+1}{4m}\pi$), QWP($\frac{\pi}{4}$). The transformations of phase shifter P(α), half-wave plate HWP(β) and quarter-wave plate QWP(γ) rotated by α , β , and γ , respectively can be written as [57]

$$U_{P(\alpha)} = \begin{pmatrix} e^{i\alpha} & 0 \\ 0 & e^{i\alpha} \end{pmatrix}, \quad (12)$$

$$U_{\text{HWP}(\beta)} = e^{i\frac{\pi}{2}} \begin{pmatrix} \cos 2\beta & \sin 2\beta \\ \sin 2\beta & -\cos 2\beta \end{pmatrix}, \quad (13)$$

$$U_{\text{QWP}(\gamma)} = \frac{1}{\sqrt{2}} \begin{pmatrix} 1 + i \cos 2\gamma & i \sin 2\gamma \\ i \sin 2\gamma & 1 - i \cos 2\gamma \end{pmatrix}. \quad (14)$$

The operations of H_{ea} and H_{eb} can be described as

$$|\uparrow\rangle \leftrightarrow \frac{1}{\sqrt{2}}(|\uparrow\rangle + |\downarrow\rangle), \quad |\downarrow\rangle \leftrightarrow \frac{1}{\sqrt{2}}(|\uparrow\rangle - |\downarrow\rangle). \quad (15)$$

The transformations of 50:50 BS can be written as

$$\begin{aligned} |R_l\rangle &\leftrightarrow \frac{1}{\sqrt{2}}(|R_l\rangle + |R_r\rangle), & |L_l\rangle &\leftrightarrow \frac{1}{\sqrt{2}}(|L_l\rangle + |L_r\rangle), \\ |R_r\rangle &\leftrightarrow \frac{1}{\sqrt{2}}(|R_l\rangle - |R_r\rangle), & |L_r\rangle &\leftrightarrow \frac{1}{\sqrt{2}}(|L_l\rangle - |L_r\rangle). \end{aligned} \quad (16)$$

Therefore, H_{ea} and H_{eb} change $|\Phi_{ep}\rangle_3$ to be

$$\begin{aligned} |\Phi_{ep}\rangle_4 &= \frac{1}{2} \cos \alpha \cos \beta |R_l^\downarrow\rangle (|\uparrow_a \uparrow_b\rangle + |\uparrow_a \downarrow_b\rangle + |\downarrow_a \uparrow_b\rangle + |\downarrow_a \downarrow_b\rangle) \\ &\quad - \frac{1}{2} \cos \alpha \sin \beta |L_r^\uparrow\rangle (|\uparrow_a \uparrow_b\rangle - |\uparrow_a \downarrow_b\rangle + |\downarrow_a \uparrow_b\rangle - |\downarrow_a \downarrow_b\rangle) \\ &\quad - \frac{1}{2} \sin \alpha \cos \beta |L_r^\uparrow\rangle (|\uparrow_a \uparrow_b\rangle + |\uparrow_a \downarrow_b\rangle - |\downarrow_a \uparrow_b\rangle - |\downarrow_a \downarrow_b\rangle) \\ &\quad + \frac{1}{2} \sin \alpha \sin \beta |R_l^\downarrow\rangle (|\uparrow_a \uparrow_b\rangle - |\uparrow_a \downarrow_b\rangle - |\downarrow_a \uparrow_b\rangle + |\downarrow_a \downarrow_b\rangle). \end{aligned} \quad (17)$$

Round_{l1}, round_{l2}, round_{r1}, and round_{r2} transform $|\Phi_{ep}\rangle_4$ into

$$\begin{aligned} |\Phi_{ep}\rangle_5 &= \frac{1}{2} \cos \alpha \cos \beta (|R_l^\downarrow\rangle |\uparrow_a \uparrow_b\rangle - |L_l^\uparrow\rangle |\uparrow_a \downarrow_b\rangle - |L_l^\uparrow\rangle |\downarrow_a \uparrow_b\rangle + |R_l^\downarrow\rangle |\downarrow_a \downarrow_b\rangle) \\ &\quad - \frac{1}{2} \cos \alpha \sin \beta (|L_r^\uparrow\rangle |\uparrow_a \uparrow_b\rangle + |R_r^\downarrow\rangle |\uparrow_a \downarrow_b\rangle - |R_r^\downarrow\rangle |\downarrow_a \uparrow_b\rangle - |L_r^\uparrow\rangle |\downarrow_a \downarrow_b\rangle) \\ &\quad - \frac{1}{2} \sin \alpha \cos \beta (|L_r^\uparrow\rangle |\uparrow_a \uparrow_b\rangle - |R_r^\downarrow\rangle |\uparrow_a \downarrow_b\rangle + |R_r^\downarrow\rangle |\downarrow_a \uparrow_b\rangle - |L_r^\uparrow\rangle |\downarrow_a \downarrow_b\rangle) \\ &\quad + \frac{1}{2} \sin \alpha \sin \beta (|R_l^\downarrow\rangle |\uparrow_a \uparrow_b\rangle + |L_l^\uparrow\rangle |\uparrow_a \downarrow_b\rangle + |L_l^\uparrow\rangle |\downarrow_a \uparrow_b\rangle + |R_l^\downarrow\rangle |\downarrow_a \downarrow_b\rangle). \end{aligned} \quad (18)$$

After S gate is applied on the right arm, $|\Phi_{ep}\rangle_5$ is projected as

$$\begin{aligned} |\Phi_{ep}\rangle_6 &= \frac{1}{2} \cos \alpha \cos \beta (|R_l^\downarrow\rangle |\uparrow_a \uparrow_b\rangle - |L_l^\uparrow\rangle |\uparrow_a \downarrow_b\rangle - |L_l^\uparrow\rangle |\downarrow_a \uparrow_b\rangle + |R_l^\downarrow\rangle |\downarrow_a \downarrow_b\rangle) \\ &\quad - \frac{1}{2} \cos \alpha \sin \beta (|L_r^\uparrow\rangle |\uparrow_a \uparrow_b\rangle + e^{i\pi/m} |R_r^\downarrow\rangle |\uparrow_a \downarrow_b\rangle - e^{i\pi/m} |R_r^\downarrow\rangle |\downarrow_a \uparrow_b\rangle - |L_r^\uparrow\rangle |\downarrow_a \downarrow_b\rangle) \\ &\quad - \frac{1}{2} \sin \alpha \cos \beta (|L_r^\uparrow\rangle |\uparrow_a \uparrow_b\rangle - e^{i\pi/m} |R_r^\downarrow\rangle |\uparrow_a \downarrow_b\rangle + e^{i\pi/m} |R_r^\downarrow\rangle |\downarrow_a \uparrow_b\rangle - |L_r^\uparrow\rangle |\downarrow_a \downarrow_b\rangle) \\ &\quad + \frac{1}{2} \sin \alpha \sin \beta (|R_l^\downarrow\rangle |\uparrow_a \uparrow_b\rangle + |L_l^\uparrow\rangle |\uparrow_a \downarrow_b\rangle + |L_l^\uparrow\rangle |\downarrow_a \uparrow_b\rangle + |R_l^\downarrow\rangle |\downarrow_a \downarrow_b\rangle). \end{aligned} \quad (19)$$

BS induces $|\Phi_{ep}\rangle_6$ to be

$$|\Phi_{ep}\rangle_7 = \frac{1}{2\sqrt{2}} \cos \alpha \cos \beta (|R_l^\downarrow\rangle |\uparrow_a \uparrow_b\rangle - |L_l^\uparrow\rangle |\uparrow_a \downarrow_b\rangle - |L_l^\uparrow\rangle |\downarrow_a \uparrow_b\rangle + |R_l^\downarrow\rangle |\downarrow_a \downarrow_b\rangle)$$

$$\begin{aligned}
 & -\frac{1}{2\sqrt{2}} \cos \alpha \sin \beta (|L_l^\uparrow\rangle |\uparrow_a \uparrow_b\rangle + e^{i\pi/m} |R_l^\downarrow\rangle |\uparrow_a \downarrow_b\rangle - e^{i\pi/m} |R_l^\downarrow\rangle |\downarrow_a \uparrow_b\rangle - |L_l^\uparrow\rangle |\downarrow_a \downarrow_b\rangle) \\
 & -\frac{1}{2\sqrt{2}} \sin \alpha \cos \beta (|L_l^\uparrow\rangle |\uparrow_a \uparrow_b\rangle - e^{i\pi/m} |R_l^\downarrow\rangle |\uparrow_a \downarrow_b\rangle + e^{i\pi/m} |R_l^\downarrow\rangle |\downarrow_a \uparrow_b\rangle - |L_l^\uparrow\rangle |\downarrow_a \downarrow_b\rangle) \\
 & +\frac{1}{2\sqrt{2}} \sin \alpha \sin \beta (|R_l^\downarrow\rangle |\uparrow_a \uparrow_b\rangle + |L_l^\uparrow\rangle |\uparrow_a \downarrow_b\rangle + |L_l^\uparrow\rangle |\downarrow_a \uparrow_b\rangle + |R_l^\downarrow\rangle |\downarrow_a \downarrow_b\rangle) \\
 & +\frac{1}{2\sqrt{2}} \cos \alpha \cos \beta (|R_r^\downarrow\rangle |\uparrow_a \uparrow_b\rangle - |L_r^\uparrow\rangle |\uparrow_a \downarrow_b\rangle - |L_r^\uparrow\rangle |\downarrow_a \uparrow_b\rangle + |R_r^\downarrow\rangle |\downarrow_a \downarrow_b\rangle) \\
 & +\frac{1}{2\sqrt{2}} \cos \alpha \sin \beta (|L_r^\uparrow\rangle |\uparrow_a \uparrow_b\rangle + e^{i\pi/m} |R_r^\downarrow\rangle |\uparrow_a \downarrow_b\rangle - e^{i\pi/m} |R_r^\downarrow\rangle |\downarrow_a \uparrow_b\rangle - |L_r^\uparrow\rangle |\downarrow_a \downarrow_b\rangle) \\
 & +\frac{1}{2\sqrt{2}} \sin \alpha \cos \beta (|L_r^\uparrow\rangle |\uparrow_a \uparrow_b\rangle - e^{i\pi/m} |R_r^\downarrow\rangle |\uparrow_a \downarrow_b\rangle + e^{i\pi/m} |R_r^\downarrow\rangle |\downarrow_a \uparrow_b\rangle - |L_r^\uparrow\rangle |\downarrow_a \downarrow_b\rangle) \\
 & +\frac{1}{2\sqrt{2}} \sin \alpha \sin \beta (|R_r^\downarrow\rangle |\uparrow_a \uparrow_b\rangle + |L_r^\uparrow\rangle |\uparrow_a \downarrow_b\rangle + |L_r^\uparrow\rangle |\downarrow_a \uparrow_b\rangle + |R_r^\downarrow\rangle |\downarrow_a \downarrow_b\rangle). \quad (20)
 \end{aligned}$$

H_{ea} and H_{eb} are performed on QD_a and QD_b again, which evolve $|\Phi_{ep}\rangle_7$ into

$$\begin{aligned}
 |\Phi_{ep}\rangle_8 = & \frac{|+l\rangle}{2} (\cos \alpha \cos \beta |\downarrow_a \downarrow_b\rangle - \cos \alpha \sin \beta (\frac{1 - e^{i\pi/m}}{2} |\uparrow_a \downarrow_b\rangle + \frac{1 + e^{i\pi/m}}{2} |\downarrow_a \uparrow_b\rangle) \\
 & - \sin \alpha \cos \beta (\frac{1 + e^{i\pi/m}}{2} |\uparrow_a \downarrow_b\rangle + \frac{1 - e^{i\pi/m}}{2} |\downarrow_a \uparrow_b\rangle) + \sin \alpha \sin \beta |\uparrow_a \uparrow_b\rangle) \\
 & + \frac{|-l\rangle}{2} (\cos \alpha \cos \beta |\uparrow_a \uparrow_b\rangle + \cos \alpha \sin \beta (\frac{1 + e^{i\pi/m}}{2} |\uparrow_a \downarrow_b\rangle + \frac{1 - e^{i\pi/m}}{2} |\downarrow_a \uparrow_b\rangle) \\
 & + \sin \alpha \cos \beta (\frac{1 - e^{i\pi/m}}{2} |\uparrow_a \downarrow_b\rangle + \frac{1 + e^{i\pi/m}}{2} |\downarrow_a \uparrow_b\rangle) + \sin \alpha \sin \beta |\downarrow_a \downarrow_b\rangle) \\
 & + \frac{|+r\rangle}{2} (\cos \alpha \cos \beta |\downarrow_a \downarrow_b\rangle + \cos \alpha \sin \beta (\frac{1 - e^{i\pi/m}}{2} |\uparrow_a \downarrow_b\rangle + \frac{1 + e^{i\pi/m}}{2} |\downarrow_a \uparrow_b\rangle) \\
 & + \sin \alpha \cos \beta (\frac{1 + e^{i\pi/m}}{2} |\uparrow_a \downarrow_b\rangle + \frac{1 - e^{i\pi/m}}{2} |\downarrow_a \uparrow_b\rangle) + \sin \alpha \sin \beta |\uparrow_a \uparrow_b\rangle) \\
 & + \frac{|-r\rangle}{2} (\cos \alpha \cos \beta |\uparrow_a \uparrow_b\rangle - \cos \alpha \sin \beta (\frac{1 + e^{i\pi/m}}{2} |\uparrow_a \downarrow_b\rangle + \frac{1 - e^{i\pi/m}}{2} |\downarrow_a \uparrow_b\rangle) \\
 & - \sin \alpha \cos \beta (\frac{1 - e^{i\pi/m}}{2} |\uparrow_a \downarrow_b\rangle + \frac{1 + e^{i\pi/m}}{2} |\downarrow_a \uparrow_b\rangle) + \sin \alpha \sin \beta |\downarrow_a \downarrow_b\rangle). \quad (21)
 \end{aligned}$$

Here $|\pm\rangle = (|R\rangle \pm |L\rangle)/\sqrt{2}$.

Lastly, we measure the outputting photon in the $\{|\pm\rangle\}$ basis, and apply some feed-forward operations on the QDs according to table 1. And then, the joint state of the whole system is collapsed into

$$\begin{aligned}
 |\Phi_e\rangle_9 = & \cos \alpha \cos \beta |\uparrow_a \uparrow_b\rangle + \cos \alpha \sin \beta (\frac{1 + e^{i\pi/m}}{2} |\uparrow_a \downarrow_b\rangle + \frac{1 - e^{i\pi/m}}{2} |\downarrow_a \uparrow_b\rangle) \\
 & + \sin \alpha \cos \beta (\frac{1 - e^{i\pi/m}}{2} |\uparrow_a \downarrow_b\rangle + \frac{1 + e^{i\pi/m}}{2} |\downarrow_a \uparrow_b\rangle) + \sin \alpha \sin \beta |\downarrow_a \downarrow_b\rangle. \quad (22)
 \end{aligned}$$

It is just the result of two-qubit (SWAP)^{1/m} gate on two electron-spin qubits a and b . That is, the quantum circuit shown in figure 2 can achieve a two-qubit (SWAP)^{1/m} gate in the two-qubit electron-spin system with a success probability of 100% in principle.

Table 1. The correlations between the outcomes of the outputting photon and the feed-forward operations for a (SWAP)^{1/m} gate with a success probability of 100% in principle. Here, $\sigma_x = |\uparrow\rangle\langle\downarrow| + |\downarrow\rangle\langle\uparrow|$, $\sigma_z = |\uparrow\rangle\langle\uparrow| - |\downarrow\rangle\langle\downarrow|$ and $I_2 = |\uparrow\rangle\langle\uparrow| + |\downarrow\rangle\langle\downarrow|$.

Detector	Feed-forward	
	QD _a	QD _b
D ₁ (+ _l)	$\sigma_z\sigma_x$	$\sigma_z\sigma_x$
D ₂ (- _l)	I_2	I_2
D ₃ (+ _r)	σ_x	σ_x
D ₄ (- _r)	σ_z	σ_z

3. Solid-state controlled-(swap)^{1/m} gate

The operation of the controlled-(swap)^{1/m} gate can be written as

$$U_{c\text{-(swap)}^{1/m}} = \begin{pmatrix} 1 & 0 & 0 & 0 & 0 & 0 & 0 & 0 \\ 0 & 1 & 0 & 0 & 0 & 0 & 0 & 0 \\ 0 & 0 & 1 & 0 & 0 & 0 & 0 & 0 \\ 0 & 0 & 0 & 1 & 0 & 0 & 0 & 0 \\ 0 & 0 & 0 & 0 & 1 & 0 & 0 & 0 \\ 0 & 0 & 0 & 0 & 0 & \frac{1+e^{i\pi/m}}{2} & \frac{1-e^{i\pi/m}}{2} & 0 \\ 0 & 0 & 0 & 0 & 0 & \frac{1-e^{i\pi/m}}{2} & \frac{1+e^{i\pi/m}}{2} & 0 \\ 0 & 0 & 0 & 0 & 0 & 0 & 0 & 1 \end{pmatrix}. \quad (23)$$

The schematic diagram for implementing an electron-spin controlled-(swap)^{1/m} gate is shown in figure 3, and it can be completed in the following five steps.

First, a single photon in the state $|R\rangle$ is injected. Based on the same arguments as made in above section, one can find that after the incident photon in the state R interacts with QD_c, HWP(- $\pi/4$), QD_{t₁} and QD_{t₂}, the system evolves from initial state

$$|\varphi_{ep}\rangle_0 = |R\rangle \otimes (\cos\alpha|\uparrow_c\rangle + \sin\alpha|\downarrow_c\rangle) \otimes (\cos\beta|\uparrow_{t_1}\rangle + \sin\beta|\downarrow_{t_1}\rangle) \otimes (\cos\delta|\uparrow_{t_2}\rangle + \sin\delta|\downarrow_{t_2}\rangle). \quad (24)$$

into

$$\begin{aligned} |\varphi_{ep}\rangle_1 = & \cos\alpha\cos\beta\cos\delta|L_r^\uparrow\rangle|\uparrow_c\uparrow_{t_1}\uparrow_{t_2}\rangle - \cos\alpha\cos\beta\sin\delta|R_r^\downarrow\rangle|\uparrow_c\uparrow_{t_1}\downarrow_{t_2}\rangle \\ & - \cos\alpha\sin\beta\cos\delta|R_r^\downarrow\rangle|\uparrow_c\downarrow_{t_1}\uparrow_{t_2}\rangle + \cos\alpha\sin\beta\sin\delta|L_r^\uparrow\rangle|\uparrow_c\downarrow_{t_1}\downarrow_{t_2}\rangle \\ & + \sin\alpha\cos\beta\cos\delta|L_l^\uparrow\rangle|\downarrow_c\uparrow_{t_1}\uparrow_{t_2}\rangle - \sin\alpha\cos\beta\sin\delta|R_l^\downarrow\rangle|\downarrow_c\uparrow_{t_1}\downarrow_{t_2}\rangle \\ & - \sin\alpha\sin\beta\cos\delta|R_l^\downarrow\rangle|\downarrow_c\downarrow_{t_1}\uparrow_{t_2}\rangle + \sin\alpha\sin\beta\sin\delta|L_l^\uparrow\rangle|\downarrow_c\downarrow_{t_1}\downarrow_{t_2}\rangle. \end{aligned} \quad (25)$$

Here, HWP(- $\pi/4$) represents a HWP set to $-\pi/4$ resulting in $-|R\rangle \leftrightarrow |L\rangle$.

Second, after H_{et_1} and H_{et_2} are performed on QD_{t₁} and QD_{t₂}, PBS₅ leads R_l^\downarrow -polarized and L_l^\uparrow -polarized components to round_{l₁}, round_{l₂}, and $S' = |R\rangle\langle R| - e^{i\pi/m}|L\rangle\langle L|$ gate in succession. While PBS₆ guides R_r^\downarrow -polarized and L_r^\uparrow -polarized components to round_{r₁}, round_{r₂} and HWP(0) continuously. Here, S' can be achieved by employing $P(\frac{1-m}{2m}\pi)$, $QWP(\frac{\pi}{4})$, $HWP(-\frac{\pi}{4m})$, $QWP(\frac{\pi}{4})$. HWP(0) realizes a $\sigma_z =$

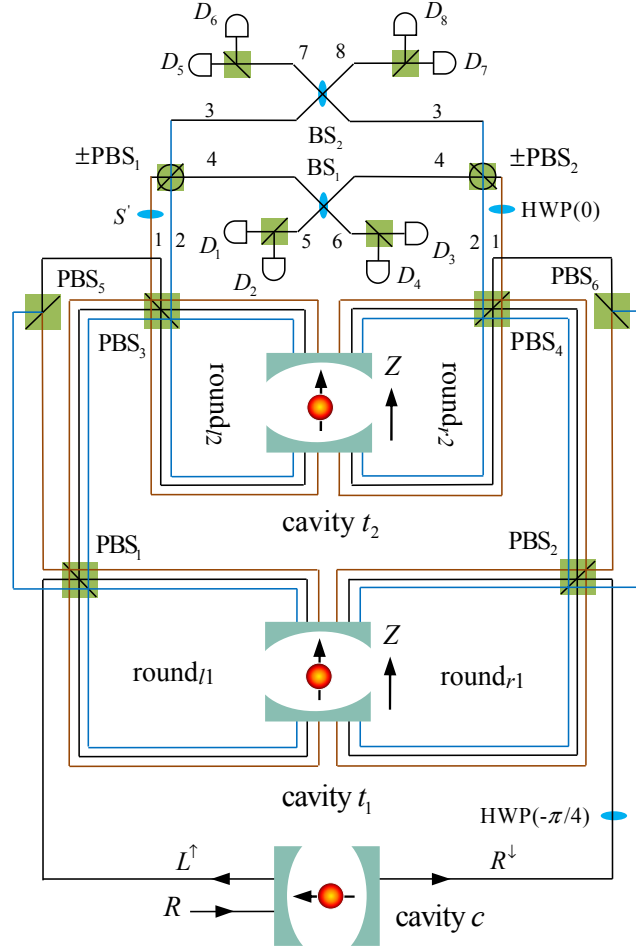


Figure 3. (Color online) Schematic diagram for the construction of a deterministic controlled-(swap)^{1/m} gate. HWP(- $\pi/4$) represents HWP oriented at $-\pi/4$ degree to complete the transformation $-|R\rangle \leftrightarrow |L\rangle$. HWP(0) indicates HWP is rotated at 0 degree performing the operation $\sigma_z = |R\rangle\langle R| - |L\rangle\langle L|$ on the passing photon. $S' = |R\rangle\langle R| - e^{i\pi/m}|L\rangle\langle L|$ denotes phase shift operation acted on the passing photon.

$|R\rangle\langle R| - |L\rangle\langle L|$ operation on the wave packets emitted from the r_1 arm. Then, $|\varphi_{ep}\rangle_1$ is changed as

$$\begin{aligned}
 |\varphi_{ep}\rangle_2 = & \frac{1}{2}(\cos \alpha \cos \beta \cos \delta |\uparrow_c\rangle(|L_{r_2}^\uparrow\rangle|\uparrow_{t_1}\uparrow_{t_2}\rangle - |R_{r_2}^\downarrow\rangle|\uparrow_{t_1}\downarrow_{t_2}\rangle - |R_{r_2}^\downarrow\rangle|\downarrow_{t_1}\uparrow_{t_2}\rangle \\
 & + |L_{r_2}^\uparrow\rangle|\downarrow_{t_1}\downarrow_{t_2}\rangle) \\
 & + \cos \alpha \cos \beta \sin \delta |\uparrow_c\rangle(-|R_{r_1}^\downarrow\rangle|\uparrow_{t_1}\uparrow_{t_2}\rangle + |L_{r_1}^\uparrow\rangle|\uparrow_{t_1}\downarrow_{t_2}\rangle - |L_{r_1}^\uparrow\rangle|\downarrow_{t_1}\uparrow_{t_2}\rangle \\
 & + |R_{r_1}^\downarrow\rangle|\downarrow_{t_1}\downarrow_{t_2}\rangle) \\
 & + \cos \alpha \sin \beta \cos \delta |\uparrow_c\rangle(-|R_{r_1}^\downarrow\rangle|\uparrow_{t_1}\uparrow_{t_2}\rangle - |L_{r_1}^\uparrow\rangle|\uparrow_{t_1}\downarrow_{t_2}\rangle + |L_{r_1}^\uparrow\rangle|\downarrow_{t_1}\uparrow_{t_2}\rangle \\
 & + |R_{r_1}^\downarrow\rangle|\downarrow_{t_1}\downarrow_{t_2}\rangle) \\
 & + \cos \alpha \sin \beta \sin \delta |\uparrow_c\rangle(|L_{r_2}^\uparrow\rangle|\uparrow_{t_1}\uparrow_{t_2}\rangle + |R_{r_2}^\downarrow\rangle|\uparrow_{t_1}\downarrow_{t_2}\rangle + |R_{r_2}^\downarrow\rangle|\downarrow_{t_1}\uparrow_{t_2}\rangle \\
 & + |L_{r_2}^\uparrow\rangle|\downarrow_{t_1}\downarrow_{t_2}\rangle)
 \end{aligned}$$

$$\begin{aligned}
 & + \sin \alpha \cos \beta \cos \delta | \downarrow_c \rangle (|L_{l_2}^\uparrow\rangle | \uparrow_{t_1} \uparrow_{t_2} \rangle - |R_{l_2}^\downarrow\rangle | \uparrow_{t_1} \downarrow_{t_2} \rangle - |R_{l_2}^\downarrow\rangle | \downarrow_{t_1} \uparrow_{t_2} \rangle \\
 & + |L_{l_2}^\uparrow\rangle | \downarrow_{t_1} \downarrow_{t_2} \rangle) \\
 & + \sin \alpha \cos \beta \sin \delta | \downarrow_c \rangle (-|R_{l_1}^\downarrow\rangle | \uparrow_{t_1} \uparrow_{t_2} \rangle + e^{i\pi/m} |L_{l_1}^\uparrow\rangle | \uparrow_{t_1} \downarrow_{t_2} \rangle - e^{i\pi/m} |L_{l_1}^\uparrow\rangle | \downarrow_{t_1} \uparrow_{t_2} \rangle \\
 & + |R_{l_1}^\downarrow\rangle | \downarrow_{t_1} \downarrow_{t_2} \rangle) \\
 & + \sin \alpha \sin \beta \cos \delta | \downarrow_c \rangle (-|R_{l_1}^\downarrow\rangle | \uparrow_{t_1} \uparrow_{t_2} \rangle - e^{i\pi/m} |L_{l_1}^\uparrow\rangle | \uparrow_{t_1} \downarrow_{t_2} \rangle + e^{i\pi/m} |L_{l_1}^\uparrow\rangle | \downarrow_{t_1} \uparrow_{t_2} \rangle \\
 & + |R_{l_1}^\downarrow\rangle | \downarrow_{t_1} \downarrow_{t_2} \rangle) \\
 & + \sin \alpha \sin \beta \sin \delta | \downarrow_c \rangle (|L_{l_2}^\uparrow\rangle | \uparrow_{t_1} \uparrow_{t_2} \rangle + |R_{l_2}^\downarrow\rangle | \uparrow_{t_1} \downarrow_{t_2} \rangle + |R_{l_2}^\downarrow\rangle | \downarrow_{t_1} \uparrow_{t_2} \rangle \\
 & + |L_{l_2}^\uparrow\rangle | \downarrow_{t_1} \downarrow_{t_2} \rangle). \tag{26}
 \end{aligned}$$

Third, after the wave packets pass through $\pm\text{PBS}_1$ and $\pm\text{PBS}_2$, Hadamard operations H_{et_1} and H_{et_2} are applied on QD_{t_1} and QD_{t_2} , respectively. Here $\pm\text{PBS}_1$, $\pm\text{PBS}_2$, H_{et_1} and H_{et_2} transform state of the system into

$$\begin{aligned}
 |\varphi_{ep}\rangle_3 = & \frac{1}{\sqrt{2}} (|+r_3\rangle \cos \alpha \cos \beta \cos \delta | \uparrow_c \downarrow_{t_1} \downarrow_{t_2} \rangle - |-r_3\rangle \cos \alpha \cos \beta \sin \delta | \uparrow_c \downarrow_{t_1} \uparrow_{t_2} \rangle \\
 & - |-r_3\rangle \cos \alpha \sin \beta \cos \delta | \uparrow_c \uparrow_{t_1} \downarrow_{t_2} \rangle + |+r_3\rangle \cos \alpha \sin \beta \sin \delta | \uparrow_c \uparrow_{t_1} \uparrow_{t_2} \rangle \\
 & - |-r_4\rangle \cos \alpha \cos \beta \cos \delta | \uparrow_c \uparrow_{t_1} \uparrow_{t_2} \rangle - |+r_4\rangle \cos \alpha \cos \beta \sin \delta | \uparrow_c \uparrow_{t_1} \downarrow_{t_2} \rangle \\
 & - |+r_4\rangle \cos \alpha \sin \beta \cos \delta | \uparrow_c \downarrow_{t_1} \uparrow_{t_2} \rangle - |-r_4\rangle \cos \alpha \sin \beta \sin \delta | \uparrow_c \downarrow_{t_1} \downarrow_{t_2} \rangle \\
 & + |+l_3\rangle \sin \alpha \cos \beta \cos \delta | \downarrow_c \downarrow_{t_1} \downarrow_{t_2} \rangle \\
 & - |-l_3\rangle \sin \alpha \cos \beta \sin \delta \left(\frac{1 - e^{i\pi/m}}{2} | \downarrow_c \uparrow_{t_1} \downarrow_{t_2} \rangle + \frac{1 + e^{i\pi/m}}{2} | \downarrow_c \downarrow_{t_1} \uparrow_{t_2} \rangle \right) \\
 & - |-l_3\rangle \sin \alpha \sin \beta \cos \delta \left(\frac{1 + e^{i\pi/m}}{2} | \downarrow_c \uparrow_{t_1} \downarrow_{t_2} \rangle + \frac{1 - e^{i\pi/m}}{2} | \downarrow_c \downarrow_{t_1} \uparrow_{t_2} \rangle \right) \\
 & + |+l_3\rangle \sin \alpha \sin \beta \sin \delta | \downarrow_c \uparrow_{t_1} \uparrow_{t_2} \rangle - |-l_4\rangle \sin \alpha \cos \beta \cos \delta | \downarrow_c \uparrow_{t_1} \uparrow_{t_2} \rangle \\
 & - |+l_4\rangle \sin \alpha \cos \beta \sin \delta \left(\frac{1 + e^{i\pi/m}}{2} | \downarrow_c \uparrow_{t_1} \downarrow_{t_2} \rangle + \frac{1 - e^{i\pi/m}}{2} | \downarrow_c \downarrow_{t_1} \uparrow_{t_2} \rangle \right) \\
 & - |+l_4\rangle \sin \alpha \sin \beta \cos \delta \left(\frac{1 - e^{i\pi/m}}{2} | \downarrow_c \uparrow_{t_1} \downarrow_{t_2} \rangle + \frac{1 + e^{i\pi/m}}{2} | \downarrow_c \downarrow_{t_1} \uparrow_{t_2} \rangle \right) \\
 & - |-l_4\rangle \sin \alpha \sin \beta \sin \delta | \downarrow_c \downarrow_{t_1} \downarrow_{t_2} \rangle). \tag{27}
 \end{aligned}$$

Fourth, after the wave packets emitted from the spatial l_4 (l_3) converge with the wave packets emitted from r_4 (r_3) at 50:50 BS_1 (BS_2), $|\varphi_{ep}\rangle_3$ is converted into

$$\begin{aligned}
 |\varphi_{ep}\rangle_4 = & \frac{1}{2} (|+7\rangle \cos \alpha \cos \beta \cos \delta | \uparrow_c \downarrow_{t_1} \downarrow_{t_2} \rangle - |-7\rangle \cos \alpha \cos \beta \sin \delta | \uparrow_c \downarrow_{t_1} \uparrow_{t_2} \rangle \\
 & - |-7\rangle \cos \alpha \sin \beta \cos \delta | \uparrow_c \uparrow_{t_1} \downarrow_{t_2} \rangle + |+7\rangle \cos \alpha \sin \beta \sin \delta | \uparrow_c \uparrow_{t_1} \uparrow_{t_2} \rangle \\
 & + |+7\rangle \sin \alpha \cos \beta \cos \delta | \downarrow_c \downarrow_{t_1} \downarrow_{t_2} \rangle \\
 & - |-7\rangle \sin \alpha \cos \beta \sin \delta \left(\frac{1 - e^{i\pi/m}}{2} | \downarrow_c \uparrow_{t_1} \downarrow_{t_2} \rangle + \frac{1 + e^{i\pi/m}}{2} | \downarrow_c \downarrow_{t_1} \uparrow_{t_2} \rangle \right) \\
 & - |-7\rangle \sin \alpha \sin \beta \cos \delta \left(\frac{1 + e^{i\pi/m}}{2} | \downarrow_c \uparrow_{t_1} \downarrow_{t_2} \rangle + \frac{1 - e^{i\pi/m}}{2} | \downarrow_c \downarrow_{t_1} \uparrow_{t_2} \rangle \right) \\
 & + |+7\rangle \sin \alpha \sin \beta \sin \delta | \downarrow_c \uparrow_{t_1} \uparrow_{t_2} \rangle - |+8\rangle \cos \alpha \cos \beta \cos \delta | \uparrow_c \downarrow_{t_1} \downarrow_{t_2} \rangle \\
 & + |-8\rangle \cos \alpha \cos \beta \sin \delta | \uparrow_c \downarrow_{t_1} \uparrow_{t_2} \rangle + |-8\rangle \cos \alpha \sin \beta \cos \delta | \uparrow_c \uparrow_{t_1} \downarrow_{t_2} \rangle \\
 & - |+8\rangle \cos \alpha \sin \beta \sin \delta | \uparrow_c \uparrow_{t_1} \uparrow_{t_2} \rangle + |+8\rangle \sin \alpha \cos \beta \cos \delta | \downarrow_c \downarrow_{t_1} \downarrow_{t_2} \rangle
 \end{aligned}$$

$$\begin{aligned}
 & -|{-}_8\rangle \sin \alpha \cos \beta \sin \delta \left(\frac{1 - e^{i\pi/m}}{2} |\downarrow_c \uparrow_{t_1} \downarrow_{t_2}\rangle + \frac{1 + e^{i\pi/m}}{2} |\downarrow_c \downarrow_{t_1} \uparrow_{t_2}\rangle \right) \\
 & -|{-}_8\rangle \sin \alpha \sin \beta \cos \delta \left(\frac{1 + e^{i\pi/m}}{2} |\downarrow_c \uparrow_{t_1} \downarrow_{t_2}\rangle + \frac{1 - e^{i\pi/m}}{2} |\downarrow_c \downarrow_{t_1} \uparrow_{t_2}\rangle \right) \\
 & +|{+}_8\rangle \sin \alpha \sin \beta \sin \delta |\downarrow_c \uparrow_{t_1} \uparrow_{t_2}\rangle - |{-}_5\rangle \cos \alpha \cos \beta \cos \delta |\uparrow_c \uparrow_{t_1} \uparrow_{t_2}\rangle \\
 & -|{+}_5\rangle \cos \alpha \cos \beta \sin \delta |\uparrow_c \uparrow_{t_1} \downarrow_{t_2}\rangle - |{+}_5\rangle \cos \alpha \sin \beta \cos \delta |\uparrow_c \downarrow_{t_1} \uparrow_{t_2}\rangle \\
 & -|{-}_5\rangle \cos \alpha \sin \beta \sin \delta |\uparrow_c \downarrow_{t_1} \downarrow_{t_2}\rangle - |{-}_5\rangle \sin \alpha \cos \beta \cos \delta |\downarrow_c \uparrow_{t_1} \uparrow_{t_2}\rangle \\
 & -|{+}_5\rangle \sin \alpha \cos \beta \sin \delta \left(\frac{1 + e^{i\pi/m}}{2} |\downarrow_c \uparrow_{t_1} \downarrow_{t_2}\rangle + \frac{1 - e^{i\pi/m}}{2} |\downarrow_c \downarrow_{t_1} \uparrow_{t_2}\rangle \right) \\
 & -|{+}_5\rangle \sin \alpha \sin \beta \cos \delta \left(\frac{1 - e^{i\pi/m}}{2} |\downarrow_c \uparrow_{t_1} \downarrow_{t_2}\rangle + \frac{1 + e^{i\pi/m}}{2} |\downarrow_c \downarrow_{t_1} \uparrow_{t_2}\rangle \right) \\
 & -|{-}_5\rangle \sin \alpha \sin \beta \sin \delta |\downarrow_c \downarrow_{t_1} \downarrow_{t_2}\rangle + |{-}_6\rangle \cos \alpha \cos \beta \cos \delta |\uparrow_c \uparrow_{t_1} \uparrow_{t_2}\rangle \\
 & +|{+}_6\rangle \cos \alpha \cos \beta \sin \delta |\uparrow_c \uparrow_{t_1} \downarrow_{t_2}\rangle + |{+}_6\rangle \cos \alpha \sin \beta \cos \delta |\uparrow_c \downarrow_{t_1} \uparrow_{t_2}\rangle \\
 & +|{-}_6\rangle \cos \alpha \sin \beta \sin \delta |\uparrow_c \downarrow_{t_1} \downarrow_{t_2}\rangle - |{-}_6\rangle \sin \alpha \cos \beta \cos \delta |\downarrow_c \uparrow_{t_1} \uparrow_{t_2}\rangle \\
 & -|{+}_6\rangle \sin \alpha \cos \beta \sin \delta \left(\frac{1 + e^{i\pi/m}}{2} |\downarrow_c \uparrow_{t_1} \downarrow_{t_2}\rangle + \frac{1 - e^{i\pi/m}}{2} |\downarrow_c \downarrow_{t_1} \uparrow_{t_2}\rangle \right) \\
 & -|{+}_6\rangle \sin \alpha \sin \beta \cos \delta \left(\frac{1 - e^{i\pi/m}}{2} |\downarrow_c \uparrow_{t_1} \downarrow_{t_2}\rangle + \frac{1 + e^{i\pi/m}}{2} |\downarrow_c \downarrow_{t_1} \uparrow_{t_2}\rangle \right) \\
 & -|{-}_6\rangle \sin \alpha \sin \beta \sin \delta |\downarrow_c \downarrow_{t_1} \downarrow_{t_2}\rangle). \tag{28}
 \end{aligned}$$

Fifth, from equation (28), one can see that after detecting the output photon in the $\{|R\rangle, |L\rangle\}$ basis and applying some proper feed-forward operations on QD_c , QD_{t_1} , and QD_{t_2} (see table 2), the state of the whole system will collapse into

$$\begin{aligned}
 |\varphi_e\rangle_5 & = \cos \alpha \cos \beta \cos \delta |\uparrow_c \uparrow_{t_1} \uparrow_{t_2}\rangle + \cos \alpha \cos \beta \sin \delta |\uparrow_c \uparrow_{t_1} \downarrow_{t_2}\rangle \\
 & + \cos \alpha \sin \beta \cos \delta |\uparrow_c \downarrow_{t_1} \uparrow_{t_2}\rangle + \cos \alpha \sin \beta \sin \delta |\uparrow_c \downarrow_{t_1} \downarrow_{t_2}\rangle \\
 & + \sin \alpha \cos \beta \cos \delta |\downarrow_c \uparrow_{t_1} \uparrow_{t_2}\rangle \\
 & + \sin \alpha \cos \beta \sin \delta \left(\frac{1 + e^{i\pi/m}}{2} |\downarrow_c \uparrow_{t_1} \downarrow_{t_2}\rangle + \frac{1 - e^{i\pi/m}}{2} |\downarrow_c \downarrow_{t_1} \uparrow_{t_2}\rangle \right) \\
 & + \sin \alpha \sin \beta \cos \delta \left(\frac{1 - e^{i\pi/m}}{2} |\downarrow_c \uparrow_{t_1} \downarrow_{t_2}\rangle + \frac{1 + e^{i\pi/m}}{2} |\downarrow_c \downarrow_{t_1} \uparrow_{t_2}\rangle \right) \\
 & + \sin \alpha \sin \beta \sin \delta |\downarrow_c \downarrow_{t_1} \downarrow_{t_2}\rangle. \tag{29}
 \end{aligned}$$

Therefore, the quantum circuit shown in figure 3 can accomplish a deterministic controlled-(swap)^{1/m} gate which implements a (SWAP)^{1/m} operation on two target QD-spin qubits if and only if the control QD-spin qubit is in the state $|\downarrow\rangle$.

4. Discussion and conclusion

In an ideal case, the photon-QD emitter will work deterministically and without any experimental errors. However, the experimental performance of the photon-cavity emitter (equation (2)) may decrease by a factor of $1 - \exp(-\tau/T_2)$ due to exciton dephasing. Here, $\tau = 1/g$ is the cavity photon lifetime (Rabi oscillation period). $T_2 \sim \mu\text{s}$ is the electron spin coherence time, which is limited by the spin-relaxation time $T_1 \sim \text{ms}$.

Table 2. The relations between the outcomes of the measurements on the photon and the feed-forward operations for a deterministic controlled-(swap)^{1/m} gate.

Detector	Feed-forward		
	QD _c	QD _{t₁}	QD _{t₂}
D_1	I_2	I_2	I_2
D_2	I_2	σ_z	σ_z
D_3	σ_z	I_2	I_2
D_4	σ_z	σ_z	σ_z
D_5	I_2	$\sigma_z\sigma_x$	$\sigma_z\sigma_x$
D_6	I_2	σ_x	σ_x
D_7	σ_z	$\sigma_z\sigma_x$	$\sigma_z\sigma_x$
D_8	σ_z	σ_x	σ_x

The optical dephasing has a slight impact on the photon-QD emitter because the optical coherence time [58] (several hundred picoseconds [59]) is ten times longer than the cavity photon lifetime τ (tens of picoseconds [60]). The hole spin coherence time ($T_2^h > 100$ ns) is three orders of magnitude longer than the cavity photon lifetime [59–61], causing the spin dephasing to be safely neglected. Moreover, the fidelity of the emitter might be reduced by a few percent as a result of the heavy-light hole mixing generated by imperfect optical selection rules [62]. Fortunately, the heavy-light hole mixing could be decreased by improving the shape, size, and type of charged exciton [63, 64]. In experiment, the coupling loss and mismatch between the photon propagating mode and the cavity mode will decrease the fidelity of the emitter. The quantum emitter loss mechanisms in the few-photon regime have been investigated, and great progress has been made in scenarios of the scattering process [65], material absorption [66], and spontaneous emissions [67].

The spin-dependent optical rules shown in equation (4) are the key ingredients in implementing our (SWAP)^{1/m} and controlled-(swap)^{1/m} gates. In practice, the imperfect birefringence and side leakage from the cavity are unavoidable in the experiment [68, 69], and they decrease the performance of the photon-QD emitter. We took into account two such imperfections with the resonant condition $\omega_{X^-} = \omega_c = \omega$; t_0 and r_0 are described by equation (3) with $g = 0$. t_0 and r_0 have opposite signs. Thus, equation (4) can be modified as

$$\begin{aligned}
 |R^\uparrow \uparrow\rangle &\rightarrow r|L^\downarrow \uparrow\rangle + t|R^\uparrow \uparrow\rangle, & |R^\uparrow \downarrow\rangle &\rightarrow t_0|R^\uparrow \downarrow\rangle + r_0|L^\downarrow \downarrow\rangle, \\
 |L^\downarrow \uparrow\rangle &\rightarrow r|R^\uparrow \uparrow\rangle + t|L^\downarrow \uparrow\rangle, & |L^\downarrow \downarrow\rangle &\rightarrow t_0|L^\downarrow \downarrow\rangle + r_0|R^\uparrow \downarrow\rangle, \\
 |L^\uparrow \downarrow\rangle &\rightarrow r|R^\downarrow \downarrow\rangle + t|L^\uparrow, \downarrow\rangle, & |R^\downarrow \uparrow\rangle &\rightarrow t_0|R^\downarrow \uparrow\rangle + r_0|L^\uparrow \uparrow\rangle, \\
 |R^\downarrow \downarrow\rangle &\rightarrow r|L^\uparrow \downarrow\rangle + t|R^\downarrow \downarrow\rangle, & |L^\uparrow \uparrow\rangle &\rightarrow t_0|L^\uparrow \uparrow\rangle + r_0|R^\downarrow \uparrow\rangle.
 \end{aligned} \tag{30}$$

To evaluate the performance of the (SWAP)^{1/m} and controlled-(swap)^{1/m} gates, we calculated the average fidelities and efficiencies of the two gates. In the experiment, the fidelity and efficiency of the gates were defined by $F = |\langle \psi_f | \psi_i \rangle|^2$ and $\eta = \frac{n_{\text{output}}}{n_{\text{input}}}$,

respectively. Here, $|\psi_i\rangle$ and $|\psi_f\rangle$ represent the ideal (equation (4)) and practical output states (equation (30)), respectively. n_{input} and n_{output} are the number of detecting photons before and after the schemes, respectively. Hence, the average fidelities and efficiencies can be written as

$$\bar{F}_{(\text{SWAP})^{1/m}} = \frac{1}{(2\pi)^2} \int_0^{2\pi} d\alpha \int_0^{2\pi} d\beta |\langle \Phi_f | \Phi_i \rangle|^2, \quad (31)$$

$$\bar{F}_{c-(\text{swap})^{1/m}} = \frac{1}{(2\pi)^3} \int_0^{2\pi} d\alpha \int_0^{2\pi} d\beta \int_0^{2\pi} d\delta |\langle \varphi_f | \varphi_i \rangle|^2, \quad (32)$$

$$\bar{\eta}_{(\text{SWAP})^{1/m}} = \frac{1}{(2\pi)^2} \int_0^{2\pi} d\alpha \int_0^{2\pi} d\beta \frac{n_{\text{output}}}{n_{\text{input}}}, \quad (33)$$

$$\bar{\eta}_{c-(\text{swap})^{1/m}} = \frac{1}{(2\pi)^3} \int_0^{2\pi} d\alpha \int_0^{2\pi} d\beta \int_0^{2\pi} d\delta \frac{n_{\text{output}}}{n_{\text{input}}}. \quad (34)$$

Without considering the coupling loss between the photon-propagating mode and the cavity mode, the average fidelities and efficiencies of the two gates are functions of g/κ and $\kappa_s/2\kappa$, respectively, and are described in figure 4 and figure 5, respectively. It is observed that the cavity side leakage, imperfect birefringence, and QD-cavity coupling strength had a great impact on the fidelities and efficiencies. When $\kappa_s \ll \kappa$, our schemes work efficiently, even in weak coupling regimes. When $\kappa_s > \kappa$ is satisfied, efficient joining schemes work only in strong coupling regimes defined by $g > (\kappa + \kappa_s)/4$. For example, $g/(\kappa + \kappa_s) = 2.7$ and $\kappa_s/\kappa = 0.05$ [70] are available, and in this case, the average fidelities of (SWAP)^{1/m} and controlled-(swap)^{1/m} gates are 99.09% and 98.93%, respectively. If $g/(\kappa + \kappa_s) = 0.5$ and $\kappa_s/\kappa = 0$, the average fidelities are approximately 89.36% and 87.42%, respectively. When $g/(\kappa + \kappa_s) = 2.5$ and $\kappa_s/\kappa = 0$, the average fidelities are approximately 99.98% and 99.97%, respectively, and the average efficiency are both over 96.13%.

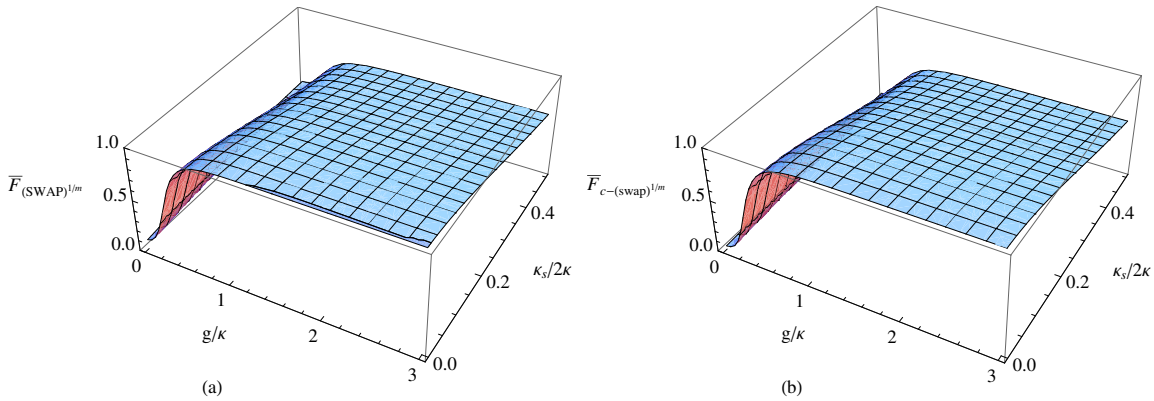


Figure 4. (Color online) The average fidelities of the two more general solid-state gates as functions of g/κ and $\kappa_s/2\kappa$. (a) The average fidelity of the (SWAP)^{1/m} gate; (b) The average fidelity of the controlled-(swap)^{1/m} gate. $w_c = \omega_{X^-} = \omega$, and $\gamma = 0.1\kappa$ are taken.

Strong coupling is a challenge in practice. Fortunately, in 2004, κ_s/κ was reduced to 0.7 with $g/(\kappa + \kappa_s) = 1$ [70–72]. The coupling strength $g/(\kappa + \kappa_s)$ was raised from 0.5 ($Q = 8800$) [70] to 2.4 ($Q = 40000$) [73] in 1.5 μm micropillar microcavities by improving the sample design, growth, and fabrication [71]. $g/(\kappa + \kappa_s) = 2.7$ was reported for a single InGaAs QD in 2012 [74]. $\kappa_s/\kappa \approx 0.2$ was reported for QD-pillar cavity in 2012 [75]. It has been reported that $\kappa_s/\kappa = 0.05$ in the strong regime could be achieved in a pillar microcavity with $Q = 9000$ [70]. As quality factor Q increases, the side leakage rate κ_s may decrease [76]. Experiments have shown that the existence of strong coupling is registered to a single QD with a coupling rate attaining to 120 meV [77, 78]. Strong coupling of QD emitters has had major breakthroughs [79]. Furthermore, coupling strength variations have been explained in diverse structures of a single QD at room temperature, which provides a possible solution for the realization of strong coupling [80].

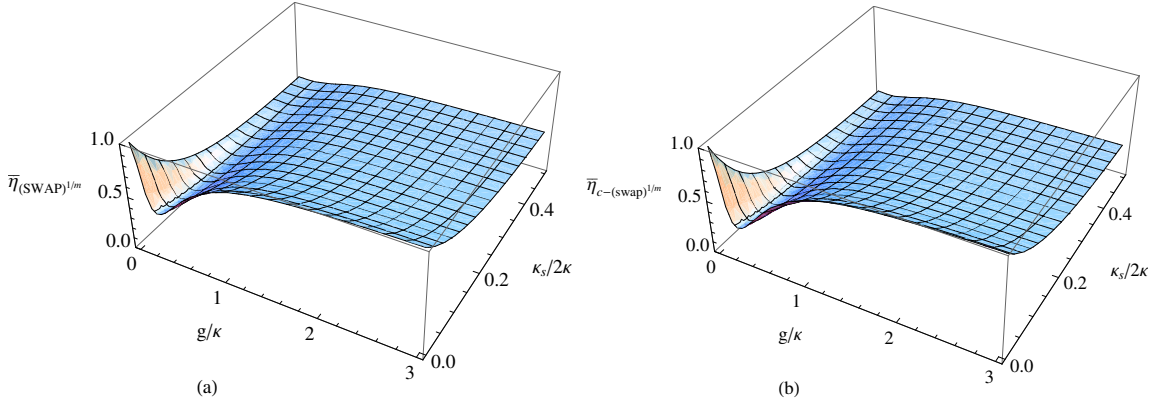


Figure 5. (Color online) The average efficiencies of the proposed two more general solid-state gates as functions of g/κ and $\kappa_s/2\kappa$. (a) The average efficiency of the (SWAP)^{1/m} gate; (b) The average efficiency of the controlled-(swap)^{1/m} gate. $w_c = \omega_{X^-} = \omega$, and $\gamma = 0.1\kappa$ are taken.

To summarize, we have proposed two deterministic schemes to implement solid-state more general (SWAP)^{1/m} and controlled-(swap)^{1/m} gates for integer $m \geq 1$. Particularly, one can obtain SWAP and Fredkin gates for $m = 1$; one can also acquire (SWAP)^{1/2} for $m = 2$. The long-distance gate qubits are bridged by flying single-photon mediate. The flexible parameter m in these gates can be adjusted by using two QWPs and one HWP. It is known that at least six photon-matter interactions are required to implement a photonic or matter SWAP gate, that the optimal synthesis of a SWAP gate is three CNOT gates [1], and that one or two photon-matter interactions are not sufficient for implementing a CNOT gate. Two parity-check gates and one additional computational qubit are necessary to implement a parity-check-based CNOT gate [81, 82]. Five two-qubit gates (four additional computational qubits) are required to synthesize a cross-Kerr-based Fredkin gate [83]. Therefore, our schemes are superior to their synthesis-based counterparts, in terms of CNOT gates [84, 85], and the cross-Kerr-based schemes [86]. Moreover, large Kerr nonlinearity is a huge challenge for the current

technology. Additional computational qubits, necessary for parity-check-based and cross-Kerr-based universal gates [87], are not required in our schemes. The evaluations of these two gates show that our schemes are feasible with current experimental technology.

Funding

This work is supported by the National Natural Science Foundation of China under Grant No. 11604012, the Fundamental Research Funds for the Central Universities under Grant No. 230201506500024.

References

- [1] Nielsen M A and Chuang I L *Quantum Computation and Quantum Information* (Cambridge University Press, Cambridge, UK, 2000).
- [2] Shor P W 1997 Polynomial-time algorithms for prime factorization and discrete logarithms on a quantum computer *SIAM J. Comput.* **26** 1484-1509
- [3] Smolin J A, Smith G and Vargo A 2013 Oversimplifying quantum factoring *Nature* **499** 163-165
- [4] Grover L K 1997 Quantum mechanics helps in searching for a needle in a haystack *Phys. Rev. Lett.* **79** 325
- [5] Figgatt C, Maslov D, Landsman K A, Linke N M, Debnath S and Monroe C 2017 Complete 3-qubit Grover search on a programmable quantum computer *Nat. Commun.* **8** 1918
- [6] Long G L 2001 Grover algorithm with zero theoretical failure rate *Phys. Rev. A* **64** 022307
- [7] Barenco A, Bennett C H, Cleve R, DiVincenzo D P, Margolus N, Shor P, Sleator T, Smolin J A and Weinfurter H 1995 Elementary gates for quantum computation *Phys. Rev. A* **52** 3457-3457
- [8] Vatan F and Williams C 2004 Optimal quantum circuits for general two-qubit gates *Phys. Rev. A* **69** 032315
- [9] Fan H, Roychowdhury V and Szkopek T 2005 Optimal two-qubit quantum circuits using exchange interactions *Phys. Rev. A* **72** 052323
- [10] Balakrishnan S and Sankaranarayanan R 2008 Entangling characterization of SWAP^{1/m} and controlled unitary gates *Phys. Rev. A* **78** 052305
- [11] Fredkin E and Toffoli T 1982 Conservative logic *Inter. J. Theor. Phys.* **21** 219-253
- [12] Ekert A and Macchiavello C 1996 Quantum error correction for communication *Phys. Rev. Lett.* **77** 2585
- [13] Holzgrafe J, Beitner J, Kara D, Knowles H S and Atatüre M 2019 Error corrected spin-state readout in a nanodiamond *npj Quantum Inform.* **5** 13
- [14] Chao R and Reichardt B W 2018 Fault-tolerant quantum computation with few qubits *npj Quantum Inform.* **4** 42
- [15] Zahedinejad E, Ghosh J and Sanders B C 2016 Designing high-fidelity single-shot three-qubit gates: A machine-learning approach *Phys. Rev. Applied* **6** 054005
- [16] Buhrman H, Cleve R, Watrous J and Wolf R D 2001 Quantum fingerprinting *Phys. Rev. Lett.* **87** 167902
- [17] Schultz C W, Wong J X H and Yu H Z 2018 Fabrication of 3D fingerprint phantoms via unconventional polycarbonate molding *Sci. Rep.* **8** 9613
- [18] Hofmann H F 2012 How weak values emerge in joint measurements on cloned quantum systems *Phys. Rev. Lett.* **109** 020408
- [19] Fiorentino M, Kim T and Wong F N C 2005 Single-photon two-qubit SWAP gate for entanglement manipulation *Phys. Rev. A* **72** 012318
- [20] Liang L and Li C 2005 Realization of quantum SWAP gate between flying and stationary qubits *Phys. Rev. A* **72** 024303

- [21] Koshino K, Ishizaka S and Nakamura Y 2010 Deterministic photon-photon $\sqrt{\text{SWAP}}$ gate using a Λ system *Phys. Rev. A* **82** 010301(R)
- [22] Wei H R and Deng F G 2015 Compact implementation of the SWAP $^\alpha$ gate on diamond nitrogen-vacancy centers coupled to resonators *Quantum Inf. Process* **82** 465-477
- [23] Bechler O, Borne A, Rosenblum S, Guendelman G, Mor O E, Netser M, Ohana T, Aqua Z, Drucker N, Finkelstein R, Lovsky Y, Bruch R, Gurovich D, Shafir E and Dayan B 2018 A passive photon-atom qubit swap operation *Nat. Phys.* **14** 996-1000
- [24] Koshino K, Inomata K, Lin Z R, Tokunaga Y, Yamamoto T and Nakamura Y 2017 Theory of deterministic entanglement generation between remote superconducting atoms *Phys. Rev. Applied* **7** 064006
- [25] Calafell I A, Cox J D, Radonjić M, Saavedra J R M, García de Abajo F J, Rozema L A and Walther P 2019 Quantum computing with graphene plasmons *npj Quantum Inform.* **5** 37
- [26] Smolin J A and DiVincenzo D P 1996 Five two-bit quantum gates are sufficient to implement the quantum Fredkin gate *Phys. Rev. A* **53** 2855
- [27] Yu N and Ying M 2015 Optimal simulation of Deutsch gates and the Fredkin gate *Phys. Rev. A* **91** 032302
- [28] Fiurášek J 2006 Linear-optics quantum Toffoli and Fredkin gates *Phys. Rev. A* **73** 062313
- [29] Fiurášek J 2008 Linear optical Fredkin gate based on partial-SWAP gate *Phys. Rev. A* **78** 032317
- [30] Gong Y X, Guo G C and Ralph T C 2008 Methods for a linear optical quantum Fredkin gate *Phys. Rev. A* **78** 012305
- [31] Wei H R and Zhu P J 2016 Implementations of two-photon four-qubit Toffoli and Fredkin gates assisted by nitrogen-vacancy centers *Sci. Rep.* **6** 35529
- [32] Ono T, Okamoto R, Tanida M, Hofmann H F and Takeuchi S 2017 Implementation of a quantum controlled-SWAP gate with photonic circuits *Sci. Rep.* **7** 45353
- [33] Liu A P, Cheng L Y, Guo Q, Zhang S and Zhao M X 2017 Universal quantum gates for hybrid system assisted by atomic ensembles embedded in double-sided optical cavities *Sci. Rep.* **7** 43675
- [34] Ren B C, Wang A H, Alsaedi A, Hayat T and Deng F G 2018 Three-photon polarization-spatial hyperparallel quantum Fredkin gate assisted by diamond nitrogen vacancy center in optical cavity *Ann. Phys.* **10** 1002
- [35] Du F F and Shi Z R 2019 Robust hybrid hyper-controlled-not gates assisted by an input-output process of low- Q cavities *Opt. Express* **27** 17493
- [36] Chen Z, Zhou Y and Shen J T 2019 Single-channel Hadamard gate by exploiting frequency conversion of single-photon Raman scattering in chiral quantum nanophotonics *Advances in Photonics of Quantum Computing, Memory, and Communication XII* **10933** 109330Z
- [37] Chen Z, Zhou Y and Shen J T 2019 Deterministic two-photon controlled phase gate by exploiting nonlinear π -phase shift in photonic molecule generations *Advances in Photonics of Quantum Computing, Memory, and Communication XII* **10933** 109330C
- [38] Shen J T and Fan S 2009 Theory of single-photon transport in a single-mode waveguide. I. coupling to a cavity containing a two-level atom *Phys. Rev. A* **79** 023837
- [39] Press D, Greve K D, McMahon P L, Ladd T D, Friess B, Schneider C, Kamp M, Höfling S, Forchel A and Yamamoto Y 2010 Ultrafast optical spin echo in a single quantum dot *Nat. Photon.* **4** 367-370
- [40] Veldhorst M, Hwang J C C, Yang C H, Leenstra A W, de Ronde B, Dehollain J P, Muhonen J T, Hudson F E, Itoh K M, Morello A and Dzurak A S 2014 An addressable quantum dot qubit with fault-tolerant control-fidelity *Nat. Nanotechnol.* **9** 98
- [41] Petta J R, Johnson A C, Taylor J M, Laird E A, Yacoby A, Lukin M D, Marcus C M, Hanson M P and Gossard A C 2005 Coherent manipulation of coupled electron spins in semiconductor quantum dots *Science* **309** 2180-2184
- [42] Berezovsky J, Mikkelsen M, Stoltz N, Coldren L and Awschalom D 2008 Picosecond coherent optical manipulation of a single electron spin in a quantum dot *Science* **320** 349-352
- [43] Carter S G, Sweeney T M, Kim M, Kim C S, Solenov D, Economou S E, Reinecke T L, Yang

- L, Bracker A S and Gammon D 2013 Quantum control of a spin qubit coupled to a photonic crystal cavity *Nat. Photon.* **7** 329-334
- [44] Pursley B C, Carter S G, Yakes M K, Bracker A S and Gammon D 2018 Picosecond pulse shaping of single photons using quantum dots *Nat. Commun.* **9** 115
- [45] Nowack K C, Koppens F H L, Nazarov Y V and Vandersypen L M K 2007 Coherent control of a single electron spin with electric fields *Science* **318** 1430-14333
- [46] Gerardot B D, Brunner D, Dalgarno P A, Ohberg P, Seidl S, Kroner M, Karrai K, Stoltz N G, Petroff P M and Warburton R J 2008 Optical pumping of a single hole spin in a quantum dot *Nature* **451** 441-445
- [47] Rakher M T, Stoltz N G, Coldren L A, Petroff P M and Bouwmeester D 2009 Externally mode-matched cavity quantum electrodynamics with charge-tunable quantum dots *Phys. Rev. Lett.* **102** 097403
- [48] Lagoudakis K G, Fischer K, Sarmiento T, Majumdar A, Rundquist A, Lu J, Bajcsy M and Vučković J 2013 Deterministically charged quantum dots in photonic crystal nanoresonators for efficient spin-photon interfaces *New J. Phys.* **15** 113056
- [49] Schneider C, Gold P, Reitzenstein S, Höfling S and Kamp M 2016 Quantum dot micropillar cavities with quality factors exceeding 250,000 *Appl. Phys. B* **122** 19
- [50] Hu C Y, Munro W J, O'Brien J L and Rarity J G 2009 Proposed entanglement beam splitter using a quantum-dot spin in a double-sided optical microcavity *Phys. Rev. B* **80** 205326
- [51] Warburton R J, Dürr C S, Karrai K, Kotthaus J P, Medeiros-Ribeiro G and Petroff P M 1997 Charged excitons in self-assembled semiconductor quantum dots *Phys. Rev. Lett.* **79** 5282-5285
- [52] Walls D F and Miburn G J *Quantum optics* (Springer-Verlag, Berlin, 1994).
- [53] Shen J T and Fan S 2007 Strongly correlated two-photon transport in a one-dimensional waveguide coupled to a two-level system *Phys. Rev. Lett.* **98** 153003
- [54] An J H, Feng M and Oh C H 2009 Quantum-information processing with a single photon by an input-output process with respect to low-*Q* cavities *Phys. Rev. A* **79** 032303
- [55] Bonato C, Haupt F, Oemrawsingh S S R, Gudat J, Ding D, Exter M P V and Bouwmeester D 2010 CNOT and Bell-state analysis in the weak-coupling cavity QED regime *Phys. Rev. Lett.* **104** 160503
- [56] Li T, Yang G J and Deng F G 2016 Heralded quantum repeater for a quantum communication network based on quantum dots embedded in optical microcavities *Phys. Rev. A* **93** 012302
- [57] Saleh B E A and Teich M C *Fundamentals of Photonics* (John Wiley and Sons, Inc., 1991).
- [58] Moody G, McDonald C, Feldman A, Harvey T, Mirin R P and Silverman K L 2016 Electronic enhancement of the exciton coherence time in charged quantum dots *Phys. Rev. Lett.* **116** 037402
- [59] Brunner D, Gerardot B D, Dalgarno P A, Karrai G K, Stoltz N G, Petroff P M and Warburton R J 2009 A coherent single-hole spin in a semiconductor *Science* **325** 70-72
- [60] Kawakami E, Scarlino P, Ward D R, Braakman F R, Savage D E, Lagally M G, Friesen M, Coppersmith S N, Eriksson M A and Vandersypen L M K 2014 Electrical control of a long-lived spin qubit in a Si/SiGe quantum dot *Nat. Nanotech.* **9** 666-670
- [61] Wachter G, Kuhn S, Minniberger S, Salter C, Asenbaum P, Millen J, Schneider M, Schalko J, Schmid U, Felgner A, Hüser D, Arndt M and Trupke M 2019 Silicon microcavity arrays with open access and a finesse of half a million *Light Sci. Appl.* **8** 37
- [62] Bester G, Nair S and Zunger A 2003 Pseudopotential calculation of the excitonic fine structure of million-atom self-assembled In_{1-x}Ga_xAs/GaAs quantum dots *Phys. Rev. B* **67** 161306
- [63] Hu C Y and Rarity J G 2011 Loss-resistant state teleportation and entanglement swapping using a quantum-dot spin in an optical microcavity *Phys. Rev. B* **83** 115303
- [64] Nemoto K, Trupke M, Devitt S J, Stephens A M, Scharfenberger B, Buczak K, Nöbauer T, Everitt M S, Schmiedmayer J and Munro W J 2014 Photonic architecture for scalable quantum information processing in diamond *Phys. Rev. X* **4** 031022
- [65] Chen Z, Zhou Y and Shen J T 2017 Exact dissipation model for arbitrary photonic Fock state transport in waveguide QED systems *Opt. Lett.* **42** 887-890

- [66] Chen Z, Zhou Y and Shen J T 2018 Entanglement-preserving approach for reservoir-induced photonic dissipation in waveguide QED systems *Phys. Rev. A* **98** 053830
- [67] Shen Y, Chen Z, He Y, Li Z and Shen J T 2018 Exact approach for spatiotemporal dynamics of spontaneous emissions in waveguide quantum electrodynamic systems *J. Opt. Soc. Am. B* **35** 607-616
- [68] Reiserer A, Kalb N, Rempe G and Ritter S 2014 A quantum gate between a flying optical photon and a single trapped atom *Nature* **508** 237-240
- [69] Reiserer A, Ritter S and Rempe G 2013 Nondestructive detection of an optical photon *Science* **342** 1349-1351
- [70] Reithmaier J P, Sek G, Löffler A, Hofmann C, Kuhn S, Reitzenstein S, Keldysh L V, Kulakovskii V D, Reinecke T L and Forchel A 2004 Strong coupling in a single quantum dot–semiconductor microcavity system *Nature* **432** 197-200
- [71] Yoshie T, Scherer A, Hendrickson J, Khitrova G, Gibbs H M, Rupper G, Ell C, Shchekin O B and Deppe D G 2004 Vacuum Rabi splitting with a single quantum dot in a photonic crystal nanocavity *Nature* **432** 200-203
- [72] Reitzenstein S, Hofmann C, Gorbunov A, Strauß M, Kwon S H, Schneider C, Löffler A, Höfling S, Kamp M and Forchel A 2007 AlAs/GaAsAlAs/GaAs micropillar cavities with quality factors exceeding 150.000 *Appl. Phys. Lett.* **90** 251109
- [73] Hu C Y, Young A, O'Brien J L, Munro W J and Rarity J G 2008 Giant optical Faraday rotation induced by a single-electron spin in a quantum dot: Applications to entangling remote spins via a single photon *Phys. Rev. B* **78** 085307
- [74] Volz T, Reinhard A, Winger M, Badolato A, Hennessy K J, Hu E L and Imamoglu A 2012 Ultrafast all-optical switching by single photons *Nat. Photonics* **6** 605
- [75] Arnold C, Demory J, Loo V, Lemaître A, Sagnes I, Glazov M, Krebs O, Voisin P, Senellart and Lanco L 2014 Macroscopic rotation of photon polarization induced by a single spin *Nat. Commun.* **6** 6236
- [76] Arnold C, Loo V, Lemaître A, Sagnes I, Krebs O, Voisin P, Senellart P and Lanco L 2012 Optical bistability in a quantum dots/micropillar device with a quality factor exceeding 200000 *Appl. Phys. Lett.* **100** 111111
- [77] Santhosh K, Bitton O, Chuntunov L and Haran G 2016 Vacuum Rabi splitting in a plasmonic cavity at the single quantum emitter limit *Nat. Commun.* **7** 11823
- [78] Chikkaraddy R, Nijs B D, Benz F, Barrow S J, Scherman O A, Rosta E, Demetriadou A, Fox P, Hess O and Baumberg J J 2016 Single-molecule strong coupling at room temperature in plasmonic nanocavities *Nature* **535** 127-130
- [79] Groß H, Hamm J M, Tufarelli T, Hess O and Hecht B 2018 Near-field strong coupling of single quantum dots *Sci. Adv.* **4** eaar4906
- [80] Leng H X, Szychowski B, Daniel M C and Pelton M 2018 Strong coupling and induced transparency at room temperature with single quantum dots and gap plasmons *Nat. Commun.* **9** 4012
- [81] Beenakker C W J, DiVincenzo D P, Emary C and Kindermann M 2004 Charge detection enables free-electron quantum computation *Phys. Rev. Lett.* **93** 020501
- [82] Nemoto K and Munro W J 2004 Nearly deterministic linear optical controlled-NOT gate *Phys. Rev. Lett.* **93** 250502
- [83] Lin Q and He B 2009 Single-photon logic gates using minimal resources *Phys. Rev. A* **80** 042310
- [84] Sleator T and Weinfurter H 1995 Realizable universal quantum logic gates *Phys. Rev. Lett.* **74** 4087
- [85] Kim T and Choi B S 2018 Efficient decomposition methods for controlled- R_n using a single ancillary qubit *Sci. Rep.* **8** 5445
- [86] Kang M S, Heo J, Choi S G, Moon S and Han S W 2019 Implementation of SWAP test for two unknown states in photons via cross-Kerr nonlinearities under decoherence effect *Sci. Rep.* **9** 6167
- [87] Luo M X, Li H R and Lai H 2016 Quantum computation based on photonic systems with two

Implementations of more general solid-state (SWAP)^{1/m} and controlled-(swap)^{1/m} gates 20

degrees of freedom assisted by the weak cross-Kerr nonlinearity *Sci. Rep.* **6** 29939